PCCP
Physical Chemistry Chemical Physics

Accepted Manuscript

This article can be cited before page numbers have been issued, to do this please use: T. Kentri, L. Kollias and S. Boghosian, *Phys. Chem. Chem. Phys.*, 2025, DOI: 10.1039/D5CP02071A.

ROYAL SOCIETY OF CHEMISTRY

rsc.li/pccp

View Article Online
DOI: 10.1039/D5CP02071A

SO_2 disproportionation for a sulphur-based thermochemical cycle studied in an *operando* Raman batch reactor

Theocharis Kentri[1], Loukas Kollias[1] and Soghomon Boghosian[1,2,*]

[1] Department of Chemical Engineering, University of Patras, GR-26500 Patras Greece

[2] Institute of Chemical Engineering Sciences, FORTH/ICE-HT, GR-26500 Patras Greece

(*) corresponding author, bogosian@chemeng.upatras.gr

Abstract

In situ and *operando* Raman spectroscopy were used to study the iodide-catalysed SO_2 disproportionation reaction at temperature of 118 °C and total pressures up to 9 bar. The disproportionation of SO_2 is one of the three process steps constituting a solar-aided thermochemical sulphur-based cycle for producing unlimitedly storable sulphur capable for on-demand consumption. A suitably designed quartz-made batch reactor cell was used enabling a special containment of SO_2, capable for *in situ* monitoring of the reaction progress in the liquid $I^-/H_2O/SO_2$ phase as well as for quantitative monitoring of the SO_2 pressure in the vapors thereof. The iodide catalyst content was varied in the 0.156 – 0.780 I^-/H_2O mol% range. The incorporation of SO_2 into the I^-/H_2O solution was facilitated by means of $O_2S...I^-$ interactions resulting in formation of $I(SO_2)_x^-$ adduct species. The rate of SO_2 consumption

was accelerated with increasing I^- content and 5% average hourly rates of SO_2 consumption could be maintained after 6 h of reaction time. The mechanistic pathway of the iodide-catalysed SO_2 disproportionation was unravelled at the molecular level. Below a certain SO_2 threshold pressure and at high I^- content, formation of the undesired I_2 by-product takes place, which is known to severely complicate the post-batch product separation. The results offer insight into the SO_2 disproportionation and are discussed with relevance to implications for its technical integration into the sulphur based solar-aided thermochemical cycle.

1. Introduction

Concentrated solar power (CSP) technology, in combination with thermal energy storage (TES) helps to secure energy supply, reduce carbon emissions, and achieve sustainable development goals.[1-4] Special attention is addressed towards renewable energy CO_2-free conversion of solar energy into medium-to-high temperature heat and/or chemicals. To this end, a three-step solar-aided thermochemical cycle based on sulphur had been suggested by General Atomics, converting solar energy into storable elemental sulphur.[3] Stored sulphur can be consumed on demand, hence the so-stored energy can be then converted back into high-temperature heat for power generation, significantly enhancing the efficiency, dispatchability, and cost-effectiveness of CSP plants.[5] The processes comprising the cycle include:

(a) the decomposition of sulphuric acid followed by SO_3 splitting

$$H_2SO_4(aq) \rightarrow H_2O(g) + SO_3(g) \qquad (450 - 500\ ^oC) \qquad (1a)$$

$$SO_3(g) \rightarrow SO_2(g) + ½\ O_2(g) \qquad (650 - 1000\ ^oC) \qquad (1b)$$

(b) the disproportionation of SO_2 with H_2O into elemental sulphur and sulphuric acid

$$3SO_2(g) + 2H_2O(l) \rightarrow 2H_2SO_4(aq) + S(s,l) \qquad (115 - 170\ ^oC) \qquad (2)$$

(c) the combustion of elemental sulphur to produce high-temperature heat and SO_2

View Article Online
DOI: 10.1039/D5CP02071A

$$S(l) + O_2(g) \rightarrow SO_2(g) \qquad (500 - 1500\ ^oC) \qquad (3)$$

The key parameters for SO_2 disproportionation include pressure, temperature, H_2O:SO_2 ratio and the catalyst system.[3] In thermodynamic grounds, the driving force of the reaction is inversely proportional to temperature, while elevated pressures are required to drive the reaction to completion, and the H_2O:SO_2 ratio needs to be controlled to avoid impeding the process. Specifically, high amount of water lowers the SO_2 partial pressure, while inadequate water content increases sulphuric acid activity at equilibrium. To the contrary, for intermediate H_2O:SO_2 ratios, the SO_2 disproportionation achieves stoichiometric formation of products (elemental sulphur and sulphuric acid), since the activity of water is high enough to drive the reaction forward, while still allowing SO_2 to remain sufficiently concentrated in the system.

The pressure dependence of the reaction remains also a key challenge, as SO_2 disproportionation only occurs above a certain threshold pressure, which varies with temperature. Experimental and modelling studies[3] have shown that with increasing temperatures, the reaction requires higher pressures to proceed efficiently. The temperature-pressure relationship is also critical, as operating at lower temperatures prevents unwanted side-reactions, e.g. H_2S formation, while increasing pressure drives forward the disproportionation reaction. An SO_2 pressure of ca. 40 bar has been found as adequate for SO_2 disproportionation to proceed smoothly in a homogeneous iodide-based catalytic batch reactor at 165 ^oC.[3] However, this temperature represents the upper limit for practical continuous reactor systems due to the increased viscosity of sulphur above this threshold, complicating extraction and pumping.[6]

Among the catalyst systems currently in use, the homogeneous iodide-based catalysts are effective in increasing the reaction rate but require complex and costly separation/recovery processing steps.[3] Catalyst recovery, especially in the case of unwanted side-product iodine

View Article Online
DOI: 10.1039/D5CP02071A

formation, requires several separation-purification steps, making the process inefficient for industrial application. Significantly, an aspect that complicates the scale-up process is balancing the pressure requirements across different steps of the thermochemical sulphur-based cycle. The sulphuric acid decomposition step (1) benefits from lower pressures for optimal SO_3 splitting, but the SO_2 disproportionation reaction (2) is favoured at higher pressures for effective SO_2 conversion to sulphur and sulphuric acid. Hence, a compromise in operating pressures is sought, as using a gas compressor in a corrosive environment is a major technical challenge.

Current knowledge of the molecular mechanisms underlying SO_2 disproportionation remains limited. Although there has been extensive research on sulphur combustion and sulphuric acid decomposition, particularly in relation to hydrogen production and concentrating solar power (CSP) applications,[7–9] the specific process of disproportionation -a fundamental reaction in the solid sulphur-based thermochemical cycle- has only been explored in laboratory scale.[3] In an attempt for fundamental understanding of the disproportionation of aqueous sulphur dioxide into sulphuric acid and elemental sulphur at room temperature,[10] chemical tests and visual observations of colour change were employed, focusing on the catalytic role of iodide ions on the reaction rate. According to this study,[10] the spontaneous disproportionation of SO_2 is thermodynamically feasible, but the reaction proceeds at an imperceptible rate without a catalyst. It is proposed that the role of the iodide ion is one of acting as an electron-transfer medium, enabling redox reactions between the sulphur species. Briefly, iodide ions likely form complexes with SO_2 (clathrates), thereby creating intermediate compounds lowering the process activation energy. Once the I^- transfers its electrons to the adsorbed SO_2, virtual iodine (I_3^-) forms, which is immediately consumed by excess SO_2. This process regenerates the iodide, allowing the catalytic cycle to continue.

View Article Online
DOI: 10.1039/D5CP02071A

The present work aims to explore the mechanism of the homogeneous iodide (I^-/H_2O)-catalysed SO_2 disproportionation. *In situ* Raman spectroscopy is applied under controlled conditions at temperatures up to 125 ^oC, SO_2 partial pressures, P_{SO_2}, up to 7 bar and total pressures up to 9.5 bar for monitoring the SO_2 consumption in the vapours and the reaction evolution in the liquid reacting system. In pursuit of this, a special containment technique has been conceived and developed to enable the spectroscopic monitoring of the process in an *operando* neoteric Raman batch reactor.

2. Experimental section

2.1 Materials, containment and sample preparation.

Sodium iodide, NaI, was from Fluka AG (p.a.). Sulphur dioxide (anhydrous, 99.98%) was from Union-Carbide and nitrogen (99.999%) was from L'Air Liquide. Triply distilled water was used for preparing the liquid mixtures. Based on the documented results of a previous work, a H_2O/SO_2 molar ratio of 2.6 was used for ensuring smooth reaction progression.[3]

The reactor cell, shown schematically in Figure 1(A) was made of quartz tubing and was suitably designed for *in situ* Raman monitoring of the SO_2 signal in the vapours and of the reaction evolution in the condensed phase (liquids, solid). The cell possessed a main bulb (~3.0-3.5 cm long, 20 mm o.d. and 17 mm i.d.) and a bottom appendix (~1 cm long, 6 mm o.d. and 4 mm i.d.) with a total volume of 7.3 cm^3. The stem used for loading the quartz cell was ~10 cm long (6 mm o.d., 4 mm i.d.). The main bulb was designed in such a way as to contain sufficient number of SO_2 moles capable of creating and withstanding an ascertained pressure of ~12 bar at ~125 ^oC after complete vaporization of SO_2, whilst the appendix had a sufficient volume to accommodate the I^-/H_2O condensed phase at an amount that fulfilled the requirement for the H_2O/SO_2 mole ratio of 2.6. The cell design, dimensions and wall thicknesses were adequate for ensuring structural integrity up to 12 bar, while providing

View Article Online
DOI: 10.1039/D5CP02071A

sufficient laser irradiation path lengths for the vapour and liquid phases (17 and 4 mm, respectively) and keeping the entire sealed optical cell within the uniform temperature zone of the vertical cylindrical core optical furnace.[11,12] Hence monitoring of *in situ* Raman spectra for both the vapour and liquid phases was enabled, the latter achieved by suitably adjusting the vertical position of the cell inside the optical furnace.

2.1.1 Containment and sample preparation. The iodide/water (I^-/H_2O) catalyst system can be formulated by using water soluble iodide salts, such as NaI, KI and NH_4I or HI. Previous laboratory tests[3] have shown that there is no significance in the iodide provenance, hence NaI was utilized. Weighed amounts of NaI were added to 1 mL of triply distilled H_2O to match the desired I^-/H_2O mol% catalyst content (Table 1) and subsequently 100 μL of the solution were introduced into the quartz cell, hence filling its bottom appendix. Afterwards, the cell was attached in a vacuum/gas-addition line shown in Figure 1(B) and evacuated while keeping the appendix containing the aqueous iodide solution immersed in liquid nitrogen. Valve 2 was then closed, to isolate the cell from the vacuum line that remained in static vacuum by closing the main valve of the vacuum pump. SO_2 was then introduced in the vacuum line up to a desired measured pressure and valve 1 was subsequently closed, thereby enclosing in the shaded T-shape glass assembly, which was confined between valve 1 and valve 2 an amount of SO_2 gas at known volume and pressure. Valve 2 is then opened and the contained SO_2 is condensed in the cell appendix which is maintained at 77 K (immersed in liquid nitrogen). Finally, valve 2 is closed and the cell is sealed-off by a propane-oxygen torch while maintaining its bottom immersed in liquid nitrogen. The amount of SO_2 added in the cell was adequate for establishing an initial pressure of $P^0_{SO_2,393\,K} = 5 - 7$ bar after complete vaporisation of SO_2. Hence, at ~125 °C the initial total cell pressure was up to ~9.5 bar, accounting also for the respective vapor pressure of H_2O (~ 2.3 bar). Table 1 compiles the characteristics of the various cells made. A reference cell containing only SO_2/H_2O was also made for comparing the Raman

View Article Online
DOI: 10.1039/D5CP02071A

spectra of the $I^-/H_2O/SO_2$ liquid systems with the counterpart spectra of iodide - free aqueous SO_2 solutions. Additionally, standard cells containing only SO_2 at known pressure were made for calibrating the $\nu_1(SO_2)$ Raman band intensity and determining the SO_2 pressure in the vapor phase over the reacting liquid mixtures. Figure S1 shows the reference SO_2 cell used.

All sealed cells containing liquid SO_2 were subjected to a 30-min crash test at 125 °C in a vertical cylindrical core furnace to confirm that they can withstand the elevated pressures (up to ~9.5 bar) without an explosion. This procedure was necessary for preventing a cell explosion from happening inside the Raman optical furnace.

2.1.2 Visual features of samples. Aqueous solutions of SO_2 at room temperature (298 K), under the SO_2 vapor pressure of ~3.5 – 4 bar, are transparent and colourless and maintain their transparent colourless feature until vaporisation of SO_2 at 125 °C ($P_{SO_2} = \sim 5 - 7$ bar). To the contrary, colourless aqueous iodide solutions obtain a bright transparent yellow colour upon SO_2 dissolution and at high iodide contents, e.g. at I^-/H_2O mol% > 0.5, split into two liquid phases in equilibrium to each other, as shown in Figure 2. The lower phase is transparent pale yellowish, and the upper phase is transparent dark yellow. As shown below (*vide infra*), the lower phase is SO_2-rich, whilst the upper phase is H_2O-rich and contains dissolved iodide and SO_2. Presumably, an electrostatic association between iodide anions and polar SO_2 molecules results in formation of $I(SO_2)_x^-$ clathrate like species,[10] hence sulphur dioxide incorporation into the liquid reacting system is promoted/facilitated by the iodide ion catalyst. Upon temperature increase to 118 °C the lower SO_2-rich phase disappears due to evaporation of SO_2.

Table 1. Characteristics for $I^-/H_2O/SO_2$ samples (iodide fraction in catalyst phase, initial pressure of SO_2)

Sample contents	Iodide fraction (I^-/H_2O), mol%	$P^0_{SO_2,393\ K}$, bar [a]
H_2O/SO_2	0	6.0
$I^-/H_2O/SO_2$	0.156	5.2

View Article Online
DOI: 10.1039/D5CP02071A

$I^-/H_2O/SO_2$	0.312	5.9
$I^-/H_2O/SO_2$	0.469	6.3
$I^-/H_2O/SO_2$	0.780	6.7
SO_2	-	8.2

[a] Determined experimentally by exploiting the Raman band intensities of the $\nu_1(SO_2)$ band.[13]

2.2 *In situ* Raman spectra and optical batch reactor

For obtaining the Raman spectra for the studied samples, each cell was placed in the optical Raman furnace[11,12] and irradiated with the green 532.0 nm line of a linearly polarized diode-pumped solid-state laser (Spectra Physics Excelsior) operated at a power level of 100 mW at the sample. The scattered light was collected at 90° through an edge filter and analysed with a ISA-Horriba IHR-320 JY monochromator. The signal was detected by a −56 °C thermoelectrically cooled CCD detector interfaced with Labspec software with a resolution of 2 cm^{-1}. With respect to the polarization configuration of the scattered light relative to the scattering horizontal plane, both VV (vertical-vertical) and VH (vertical- horizontal) configurations were applied. The observed wavenumbers' precision and depolarisation ratios were calibrated by recording spectra of a CCl_4 standard sample. Further details concerning the Raman spectroscopy set up are described earlier.[14] Notably, the use of a 100-mW power for the incident laser radiation does not raise concerns for sample overheating, because of the continuous movement of the molecules comprising the liquid and/or the gaseous phase, thereby resulting in a continuous renewal of the sample of molecules being irradiated. Hence, in each instant the temperature of the irradiated sample can safely be taken equal to the temperature of the container, like if a kind of rotating-sample technique[15] was utilised.

Each cell, before being inserted in the Raman optical furnace, was first tested for 30 minutes at 125 °C in a tube furnace to confirm that it can withstand the inner pressure. Initial spectra were recorded at 25°C, followed by heating up to 118°C, where Raman spectra were

View Article Online
DOI: 10.1039/D5CP02071A

obtained for both the vapours and the liquid phase, and the reaction progress was monitored spectroscopically for ca. 10 h. After stopping the reaction or after reaction completion (the latter evidenced by iodine formation), the cell was cooled to 25°C, and Raman spectra of the vapor and liquid phases were obtained. Cells where the reaction had not been completed were stored at room temperature and progress in the SO_2 disproportionation could be monitored by intermittently recording Raman spectra at room temperature for several weeks, thereby observing accumulation of solid sulphur product in the cell appendix bottom.

Raman spectroscopy can be used for determining the pressure of a gas (*i.e.* SO_2, $P_{SO_2}|_{cell\,i}$) in a reaction mixture sample contained in a Raman cell at a temperature T_i by comparing the intensity of a band (integrated peak area, $I_{SO_2}|_{cell\,i}$) representing the species of interest (*i.e.* $\nu_1(SO_2)$) with the intensity (integrated peak area) of the same band in a reference cell ($I_{SO_2}|_{\mathrm{R}}$) containing only SO_2 at a known pressure, $P_{SO_2}|_{\mathrm{R}}$, and temperature, T_{R}.[13] The calculation is based in the following formula[13]

$$P_{SO_2}|_{cell\,i} = I_{SO_2}|_{cell\,i} \cdot \frac{P_{SO_2}|_{\mathrm{R}}}{I_{SO_2}|_{\mathrm{R}}} \cdot \frac{T_i}{T_{\mathrm{R}}} \cdot \frac{1 - \exp\left(-\frac{hc\nu_1(SO_2)}{kT_i}\right)}{1 - \exp\left(-\frac{hc\nu_1(SO_2)}{kT_{\mathrm{R}}}\right)} \qquad (4)$$

where h, c and k are Planck's constant, the velocity of light and the Boltzmann's constant, respectively. The reference measurement took place several times for SO_2 vapors in equilibrium with liquid SO_2 at 16 °C ($T_{\mathrm{R}} = 289$ K) and the corresponding SO_2 vapor pressure used was 2.93 bar ($P_{SO_2}|_{\mathrm{R}} = 2.89$ bar).[16]

Hence, the vapor Raman spectra were exploited for quantitative monitoring of the partial pressure of SO_2 above the liquid catalyst/reaction mixture. To this end, during the present work the spectral recording conditions and the optical geometry remained unchanged. The quartz Raman cells inserted in the Raman furnace were kept in fixed position relative to the optics. Indicatively, the SO_2-containing standard cells used for relating the $\nu_1(SO_2)$ band intensity in the gas phase to the partial pressure of SO_2 above the liquid catalyst/reaction

View Article Online
DOI: 10.1039/D5CP02071A

mixture could be removed from the furnace, cooled and subsequently reintroduced in the furnace and the measured intensities were reproduced to within 5%.

3. Results and Discussion

3.1 Raman spectra of the $I^-/H_2O/SO_2$ liquid system at room temperature.

Figure 3 shows Raman spectra of the $I^-/H_2O/SO_2$ liquid catalyst/reaction mixture at room temperature obtained for various I^-/H_2O mol% values in the 0 – 0.780 range in equilibrium with gaseous SO_2 (see experimental section). Polarised (VV) and depolarised (VH) spectra are displayed for commenting on the polarisation characteristics of the featured bands. In absence of iodide ions, *i.e.* in the H_2O-SO_2 liquid system, SO_2 is known to form various hydrates with water[17] that slightly perturb its symmetry. Hence, as shown in spectrum Fig. 3(a), SO_2 maintains *mutatis mutandis* its symmetric structural configuration with a polarised band at 1155 cm^{-1} due to the symmetric ν_1 stretching mode, which exhibits a depolarization ratio of $\rho = \sim 0.10$, due to the perturbations caused within the solution. When iodide ions are present, part of the SO_2 molecules form $I(SO_2)_x^-$ clathrate-like or adduct species via $O_2S\ldots I^-$ interactions,[10,18] in which the SO_2 moiety is distorted in such a way as to cause a slight elongation of the S–O bonds, thereby justifying a red shift, and a further perturbation of its symmetry, by that means affecting the polarisation characteristics of its main stretch. Remarkably, due to the $O_2S\ldots I^-$ interactions, the ν_1 mode shifts to 1144 cm^{-1} and its depolarisation ratio is increased (see e.g. spectrum (d) in Fig. 3). Hence, with increasing I^-/H_2O mol%, more SO_2 molecules participate in $O_2S\ldots I^-$ interactions, as seen in spectra (b) – (d) shown Fig. 3. Moreover, for I^-/H_2O mol%, > 0.500, the $I^-/H_2O/SO_2$ liquid splits into two conjugate phases in equilibrium (see Fig. 2), of which the lower-density upper phase is an iodide solution-rich one with a Raman spectrum shown in Fig. 3(d) and the higher density lower phase is an SO_2-rich one with a Raman spectrum shown in Fig. 3 inset, which also

View Article Online
DOI: 10.1039/D5CP02071A

includes the Raman spectrum of the lower density upper phase for comparison. It turns out that the incorporation of SO_2 into the liquid catalyst/reacting mixture is facilitated by the presence of I^- ions by means of $O_2S\ldots I^-$ interactions, as evidenced by the Raman spectra.

3.2 Monitoring the iodide – catalysed homogeneous SO_2 disproportionation by *in situ* Raman spectroscopy of the liquid reaction mixture at 118 °C.

Figure 4 pertains to the liquid-gas $I^-/H_2O/SO_2(l) – SO_2(g)$ system with I^-/H_2O = 0.156 mol% and shows two snapshots of the liquid Raman spectra. Trace 4(a) is obtained for the liquid mixture at 25 °C, *i.e.* before heating up the Raman furnace for initiating the reaction. Notably, prior to inserting in the Raman furnace, the quartz reaction cell has been subjected to a 30 min "crash test" at 125 °C. Hence, the strongest HSO_4^- mode at 1054 cm^{-1} can already be discerned in spectrum Fig. 4(a), thereby indicating the initiation of the SO_2 disproportionation reaction, already during the 30 min "crash test". Spectrum Fig. 4(b) is obtained at 118 °C after 9.75 h of reaction time and exhibits: (a) the $\nu_1(SO_2)$ mode, which is weakened due to vaporisation (thereby increasing the cell pressure) and consumption of SO_2 due to the disproportionation reaction; and (b) additional emerging bands at 1195 cm^{-1} (weak), 1054 cm^{-1} (strong), 878 cm^{-1} (medium), 592 cm^{-1} (medium) and 425 cm^{-1} (medium) due to $HSO_4^-(aq)$[19,20] and at 475 and 220 cm^{-1} due to elemental sulphur[21] produced as a result of the SO_2 disproportionation reaction.

Figure 5 shows the evolution of the SO_2 disproportionation reaction in the liquid phase, monitored in the *in situ* Raman batch reactor at 118 °C for two different contents of iodide catalyst. Panel 5(A) shows the evolution in the time span 0.75 – 9.75 h for I^-/H_2O = 0.156 mol% and Panel 5(B) shows the respective evolution up to 6 h for I^-/H_2O = 0.780 mol%. As evidenced from the intensity of the 1054 cm^{-1} HSO_4^- band relative to the 1154 cm^{-1} "SO_2" band envelope,

View Article Online
DOI: 10.1039/D5CP02071A

the disproportionation reaction proceeds much faster when increasing the content of the iodide catalyst. Notably, spectra pertaining to "t=0.75 h" in Fig. 5 exhibit in both panels bands due to the HSO_4^- produced during the 30 min "crash test" taken place at 125 °C before insertion of each reactor cell into the Raman furnace.

The SO_2 disproportionation reaction proceeds in the liquid phase via formation of $HSO_4^-(aq)$, catalysed by I^- in two steps: one of a reduction and one of an oxidation according to the following mechanistic scheme, which is slightly modified compared to a previously proposed one:[10]

SO_2 "Dissolution":

$$3SO_2(g) \rightarrow 3SO_2(aq)$$

Reduction step:

$$SO_2(aq) + 6I^-(aq) + 4H_3O^+(aq) \rightarrow S(s) + 2I_3^-(aq) + 6H_2O \quad (5)$$

Oxidation step:

$$2SO_2(aq) + 2I_3^-(aq) + 10H_2O(l) \rightarrow 2HSO_4^-(aq) + 6I^-(aq) + 6H_3O^+(aq) \quad (6)$$

Total disproportionation reaction:

$$3SO_2(g) + 4H_2O(l) \rightarrow 2HSO_4^-(aq) + S(s) + 2H_3O^+(aq) \quad (7)$$

A follow-up step pertaining to $HSO_4^-(aq)$ ionization converts part of $HSO_4^-(aq)$ to $SO_4^{2-}(aq)$ upon cooling[18] from the reaction temperature of 118 °C to 25 °C where both ions remain in equilibrium:

$$2HSO_4^-(aq) + 2H_2O(l) \leftrightarrow 2SO_4^{2-}(aq) + 2H_3O^+(aq) \quad (8)$$

The I^- ion is Raman silent, whilst the short-living I_3^- iodide intermediate, which has a characteristic Raman stretching vibration at 114 cm^{-1},[22] is not detectable, as its extent of presence is below the detection limit. Hence, neither elemental iodine, I_2, nor its I_3^- form are

View Article Online
DOI: 10.1039/D5CP02071A

detected as long as the reaction proceeds. Actually, I_3^- is consumed at the very instant of its formation. The Bunsen reaction

$$SO_2(g) + 2H_2O(l) + I_2(s,l) \leftrightarrow 2HI(aq) + H_2SO_4(aq) \quad (9)$$

remains shifted to the right as long as the residual SO_2 pressure remains above a certain threshold value, thereby preventing the undesired formation of I_2. Interestingly, in the following section, when increasing the I^-/H_2O mol% ratio in the 0.156 – 0.469 range, the reaction takes place with an increasing rate of SO_2 consumption up to 9.75 h of typically applied daily reaction time, and is thereafter stopped by cooling the furnace. However, when a 0.780 I^-/H_2O mol% ratio is used, the reaction proceeds much faster and is terminated abruptly because reaction (9) shifts to the left and formation of iodine, $I_2(l,g)$ and $I_3^-(aq)$ is detected in the *in situ* Raman batch quartz reactor (*vide infra)*. The progress duration of the disproportionation reaction before the undesired iodine (I_2) appearance depends on the initial pressure of SO_2 in the batch reactor cell as well as the iodide (I^-) content, in accordance with the Bunsen reaction (9).

3.3 *Operando* Raman monitoring of the SO_2 pressure decay in the gas phase during SO_2 disproportionation catalysed by I^-/H_2O at 118 °C and reaction outcome.

3.3.1 Low-to-medium iodide catalyst content. Figure 6 portrays the vapor Raman spectra obtained over the reacting $H_2O/\ SO_2/\ I^-$ liquid and shows the decay of the main gaseous SO_2 symmetric stretching mode band, $\nu_1(SO_2)$, vs time by showing sequential snapshots of the vapor Raman spectra in the t = 0.75 – 10 h span for the reaction batches that used 0.156 I^-/H_2O mol% (Panel 6(A)), 0.312 I^-/H_2O mol% (Panel 6(B)) and 0.469 I^-/H_2O mol% (Panel 6(C)). The corresponding dependence of the SO_2 pressure as a function of reaction time for each reacting mixture in the 0.156 – 0.469 I^-/H_2O mol% range, calculated using eq (4), is

displayed in plots (a) – (c) shown in Figure 7(A). It is evident that the SO_2 pressure decay as a function of reaction time is steeper when higher amounts of iodide catalyst are present. The SO_2 pressure data can furthermore be exploited to calculate the percent average hourly SO_2 consumption rates and the results are displayed in plots (a), (b) and (c) shown in Figure 7(B). Whereas an average 1% hourly SO_2 consumption rate is calculated for the reaction batch with the lowest 0.156 I^-/H_2O mol% content, initial hourly rates of 4.0 to 4.7% are achieved with 0.312 and 0.469 I^-/H_2O mol%. Significantly, a ~3% hourly SO_2 consumption rate is maintained after *ca.* 9 h of reaction for an iodide content of 0.469 I^-/H_2O mol%.

In all three cases of low-to-medium iodide catalyst content (*i.e.* 0.156 – 0.469 I^-/H_2O mol%) the SO_2 disproportionation reaction proceeds with SO_2 consumption and HSO_4^- production as shown in Figure 5(A) pertaining to the low 0.156 I^-/H_2O mol% content as well as formation of S(s,l) identified by the characteristic 153, 222 and 475 cm^{-1} bands due to sulphur as seen in Figure S2 portraying the full wavenumber range of the Raman spectrum obtained for the $H_2O/\ SO_2/\ I^-/HSO_4^-$ reacting liquid mixture at 118 °C. Notably, part of the sulphur occurs in solid form and is settled in the bottom cell appendix where temperature is very close to the melting point of 116°C, hence whereas the reaction progress can be followed by the gradual increase of the HSO_4^- bands there is no commensurate increase of the bands due to sulphur. In all above cases (*i.e.* 0.156 – 0.469 I^-/H_2O mol%) the reaction proceeds without formation of the undesired side product iodine, I_2, that could be formed by the reverse Bunsen reaction (9) if the relative amounts of SO_2, I^- and HSO_4^- would allow reaction (9) to be shifted to the left. Hence, SO_2 is consumed, as shown in Fig. 6(a,b,c) and HSO_4^- is produced (Fig. 5(A)) without iodine formation for 10 h of reaction time, after which the experiments were terminated and the Raman batch reactor cooled to room temperature. Visual inspection of the reactor cell after cooling reveals the occurrence of a yellow solid chunk precipitate at the bottom of the cell appendix, as shown in Figure 8(A). Figure 8(B) shows the reactor cell

View Article Online
DOI: 10.1039/D5CP02071A

through the scattering window inside the Raman furnace, where the solid chunk glows being irradiated by the 532 nm laser at a very low power of 5 mW. Hence, to validate that the yellow solid chunk is the desired sulphur product, a Raman spectrum of the solid chunk contained inside the $H_2O/\ SO_2/\ I^-/HSO_4^-$ liquid mixture was recorded and shown in Fig. 8(C). The spectrum shown in Fig. 8(C) consists exclusively of the well-known Raman bands at 222, 246, 439 and 475 cm^{-1} due to S(s).[21]

Interestingly, when the reactor cell is cooled to room temperature (after ca 10 h of reaction at 118 – 123 ^oC), the SO_2 disproportionation continues to proceed. This is quite reasonable on account of the thermodynamics of reaction (7):

$$3SO_2(g) + 4H_2O(l) \rightarrow 2HSO_4^-(aq) + S(s) + 2H_3O^+(aq) \quad (7)$$

$$\Delta G^0_{298\ \mathrm{K}} = -136.99\ \mathrm{kJ\ mol^{-1}}, \quad \Delta H^0_{298\ \mathrm{K}} = -312.53\ \mathrm{kJ\ mol^{-1}}$$

where the negative Gibbs free energy implies that the reaction is thermodynamically favoured at room temperature, albeit at low intrinsic rates. This can be seen in Figure 9, showing Raman snapshots obtained at room temperature for the reactor cell with 0.312 I^-/H_2O mol% right after the 30 min crash test (trace (a)), after 9.75 h of reaction at 118 ^oC (trace (b)) and after 32 days on shelf (trace (c)), which shows a very high extent of reaction, *i.e.*by exhibiting strong bands due to HSO_4^-, a prominent band due to the strongest (symmetric stretch) of SO_4^{2-} and strong bands due to S(s) suspended in the liquid phase.

3.3.2 High iodide catalyst content. When a higher catalyst content of 0.780 I^-/H_2O mol% was used, the SO_2 pressure decay is even steeper as displayed in plot (d) shown in Fig. 7(A) and the pertinent percent hourly SO_2 consumption rates are shown in plot (d) in Fig. 7(B). Initial hourly rates of 6% could be achieved, decaying to 4.7% after *ca.* 7 h of reaction time. Significantly, as shown in Figure 10(A), after 7 h of reaction time, the SO_2 signal fell abruptly

View Article Online
DOI: 10.1039/D5CP02071A

and new strong bands emerged in the vapor Raman spectrum exhibiting vibrational-rotational structure, which is reminiscent of bands due to iodine vapors, $I_2(g)$. The occurrence of the deep purple coloured iodine vapours justifies the abrupt fall of the SO_2 signal in plot (d) shown in Fig. 7(A). Indeed, recording of the Raman spectrum of vapors in the 150 – 1600 cm^{-1} after 9 h resulted in the well-known resonance Raman spectrum of iodine vapors[23] showing a progression of multiple overtones of the 214 cm^{-1} vibrational fundamental with each overtone exhibiting fine vibrational-rotational structure and the spectrum is shown in Figure 10(B) (red trace (a)). By lifting the cell inside the Raman furnace and irradiating the liquid phase contained in the cell appendix, the Raman spectrum of the liquid mixture after 10 h could be recorded (blue trace (b) in Figure 10(B)). The cell was then removed from the Raman furnace for inspection and the characteristic purple color of iodine vapors could be observed (Figure 10(C)). Moreover, the solid sulphur chunk at the bottom of the cell appendix had a very dark purple color due to its interaction with iodine.

The fast disproportionation of SO_2 when a high catalyst content of 0.780 I^-/H_2O mol% is used, results in stoichiometrically commensurate production of HSO_4^-, which in combination with the high I^- content shifts the Bunsen reaction (9) to the left, thereby accounting for formation of iodine. After cooling the reactor cell to room temperature, the dark liquid phase is largely decolorised due to combination of $I^-(aq)$ with iodine to form the triiodide ion $I_3^-(aq)$, as shown in Figure 10(D), showing the Raman spectrum of the liquid over the solid $S(s)/I_2(l)$chunk where a band at 114 cm^{-1} characteristic of the $I_3^-(aq)$ vibrational mode[22] is observed. Additionally, strong features due to $HSO_4^-(aq)$ formed according to reaction (7) are observed together with the most characteristic $\nu_1(A_1)$ stretching mode of $SO_4^{2-}(aq)$ formed according to equilibrium (8) and the ν_1 mode of the SO_2 remaining in the liquid mixture.

3.4 Implications for the sulphur-based thermochemical cycle

View Article Online
DOI: 10.1039/D5CP02071A

An innovative methodology for understanding the mechanistic route for the benchmark homogeneous iodide-catalysed SO_2 disproportionation based on *in situ* molecular spectroscopy and for monitoring the process is established. By *in situ* monitoring of the process, in particular the SO_2 pressure, prevention of the undesired iodine by-product formation can be achieved. The laboratory results indicate that whereas an increase of the I^-/H_2O ratio accelerates on one hand the reaction, a high I^- content combined with a low threshold SO_2 pressure may on the other hand lead to undesired I_2 formation. Intermittent SO_2 replenishment may prolong the progress of the reaction, thereby avoiding the technically challenging post-batch sulphur-iodine separation. The laboratory tests show that for a I^-/H_2O ratio below 0.500 mol% a SO_2 pressure of 4.7 bar is adequate for preventing formation of I_2.

The hourly SO_2 consumption rates of 5% after 6 h of reaction time at the mild conditions of 118 ^oC and total pressures below 9 bar are quite promising for achieving a technically sought compromise between the sulphuric acid decomposition step (reactions (1a),(1b)), which precedes the SO_2 disproportionation step (reaction (2)) in the solar-aided sulphur-based thermochemical cycle, thereby avoiding the use of a gas compressor in a corrosive environment.

4. Conclusions

An unprecedented *operando* Raman spectroscopic study of the benchmark process of homogeneous iodide-catalysed SO_2 disproportionation has been undertaken at a temperature of 118 ^oC and pressures up to 9 bar. A suitably designed neoteric quartz batch reactor cell was used, enabling *in situ* monitoring of the reaction progress in the homogeneous liquid reacting phase as well as *in situ* quantitative monitoring of SO_2 consumption in the vapors thereof.

View Article Online
DOI: 10.1039/D5CP02071A

The mechanistic pathway of the I^- – catalysed SO_2 disproportionation under mild conditions, specifically at 118 °C and total pressure (gaseous SO_2 and H_2O vapors) of ~9 bar is deciphered at the molecular level. The incorporation of SO_2 in the I^-/H_2O solution is facilitated by means of $I(SO_2)_x^-$ clathrate-like or adduct species formed via $O_2S\ldots I^-$ interactions in the liquid state. The SO_2 disproportionation reaction mechanism consists of two main steps, one of a reduction resulting in formation of sulphur and of a short living $I_3^-(aq)$ intermediate and one of an oxidation resulting in formation of $HSO_4^-(aq)$, which upon cooling converts to sulphuric acid.

The rate of SO_2 consumption, measured by exploiting the Raman band intensity measurements, is accelerated with increasing content of the I^- catalyst, in the range 0.156 – 0.780 I^-/H_2O mol%, up to a certain limit, beyond which the lowered SO_2 presence, the high I^- content and HSO_4^- accumulation result in formation of the undesired iodine by-product by means of the reverse Bunsen reaction, thereby terminating the SO_2 disproportionation reaction. There is an apparent SO_2 pressure low threshold, which in combination with a high I^- content terminates the reaction, implying that a best compromise between the two is to be sought. Therefore, a continuous monitoring of the SO_2 pressure and intermittent replenishments with SO_2 would allow the controlled duration of batch operations at technical level. By that means the formation of iodine could be avoided and hence the required number of post-batch purification steps could be reduced. Most importantly, the technically utmost problematic separation step, *i.e.* the one of sulphur-iodine separation could be avoided.

Data availability

The data supporting this work are included in the main article and its Supplementary Information.

View Article Online
DOI: 10.1039/D5CP02071A

Conflicts of Interest

There are no conflicts of interest to declare.

Acknowledgment. This project has received funding from the European Union's European Innovation Council and SMEs Executive Agency (EISMEA) programme under grant agreement no 101115538 - SULPHURREAL.

References

1. S. J. Wagner and E. S. Rubin, Economic Implications of Thermal Energy Storage for Concentrated Solar Thermal Power, *Renewable Energy*, 2014, **61**, 81–95.

2. P. Denholm, Y. H. Wan, M. Hummon and M. Mehos, The Value of CSP with Thermal Energy Storage in the Western United States. *Energy Procedia* 2014, **49**, 1622-1631.

3. B. Wong, L. Brown, R. Buckingham, W. Sweet, B. Russ and M. Gorensek, Sulfur Dioxide Disproportionation for Sulfur Based Thermochemical Energy Storage, *Sol. Energy*, 2015, **118**, 134-144.

4. O. Achkari and A. El Fadar, Latest Developments on TES And CSP Technologies – Energy and Environmental Issues, Applications and Research Trends, *Appl. Therm. Eng.*, 2020, **167**, 114806.

5. K. Yagi, R. Sioshansi and P. Denholm, Evaluating a Concentrating Solar Power Plant as An Extended-Duration Peaking Resource, *Sol. Energy*, 2019, **191**, 686-696.

6. T. Doi, *Rev. Phys. Chem. Jpn.*, 2016, **33**, 1–23.

7. A. Noglik, M. Roeb, C. Sattler and R. Pitz-Paal, Experimental Study on Sulfur Trioxide Decomposition in a Volumetric Solar Receiver-Reactor, *Int. J. Energy Res.*, 2009, **33**, 799-812.

8. C. S. Kim, S.-D. Hong, Y.-W.Kim, J.-H. Kim, W. J. Lee and J. Chang, Thermal Design of a Laboratory-Scale SO_3 Decomposer for Nuclear Hydrogen Production, *Int. J. Hydrogen Energy*, 2008, **33**, 3688-3699.

9. A. Terada, J. Iwatsuki, S. Ishikura, H. Noguchi, S. Kubo, H. Okuda, S. Kasahara, N. Tanaka, H. Ota, K. Onuki and R. Hino, Development of Hydrogen Production Technology by Thermochemical Water Splitting IS Process Pilot Test Plan, *J. Nucl. Sci. Technol.*, 2007, **44**, 477-482.

10. V. M. Petruševski, M. Bukleski and M. Stojanovsk, On the Catalyzed Disproportionation of SO_2 in Aqueous Solution of KI: A Marathon Classroom Demonstration, *J. Lab. Chem. Educ.*, 2013 **1**, 1–4.

11. S. Boghosian, Vibrational Modes and Structure of Vanadium(V) Complexes in M_2SO_4-V_2O_5 (M = K Or Cs) Molten Salt Mixtures, *J. Chem. Soc., Faraday Trans.*, 1998, **94**, 3463-3469.

12. S. Boghosian, A. Chrissanthopoulos and R. Fehrmann, Structure of Vanadium Oxosulfato Complexes in V_2O_5-$M_2S_2O_7$-M_2SO_4 (M = K, Cs) Melts. A High Temperature Spectroscopic Study, *J. Phys. Chem. B*, 2002, **106**, 49-56.

13. S. Boghosian and G. N. Papatheodorou, Evaluation of Stoichiometric Coefficients and Thermodynamic Functions of Vapor Complexes Using Raman Spectroscopy: The Systems ZrX_4-AlX_3 (X = Br, Cl), *J. Phys. Chem.*, 1989, **93**, 415-421.

14. A. G. Kalampounias and S. Boghosian, Distribution Of Tellurite Polymorphs in the xM_2O-(1 - x)TeO_2 (M = Li, Na, K, Cs, and Rb) Binary Glasses Using Raman Spectroscopy, *Vib. Spectrosc.* 2012, **59**, 18-22.

15. S. Boghosian, G. A. Voyiatzis and G. N. Papatheodorou, Gas-Phase, Liquid and Solid Complexes in the $POCl_3$-$FeCl_3$ System, *J. Chem. Soc., Dalton Trans*., 1996, 3405 - 3410,

16. D. R. Stull, Vapor Pressure of Pure Substances. Organic and Inorganic Compounds, *Ind. Eng. Chem.*, 1947, **39**, 517-540.

17. N. N. Greenwood and A. Earnshaw, *Chemistry of the Elements*, 2nd ed. Oxford, UK: Butterworth-Heineman, 1998, pp 700-701.

18. F. Dankert, A. Feyh and C. von Hänisch, Chalcogen Bonding of SO_2 and s-Block Metal Iodides Near Room Temperature: A Remarkable Structural Diversity, *Eur. J. Inorg. Chem*. 2020, 2744–2756

19. C. E. Lund Myhre, D. H. Christensen, F. M. Nicolaisen and C. J. Nielsen, Spectroscopic Study of Aqueous H_2SO_4 at Different Temperatures and Compositions: Variations in Dissociation and Optical Properties*, J. Phys. Chem. A* 2003, **107**, 1979-1991.

20. C. B. Knudsen, A.G. Kalampounias, R. Fehrmann and S. Boghosian, Thermal Dissociation of Molten $KHSO_4$: Temperature Dependence of Raman Spectra and Thermodynamics, *J. Phys. Chem. B*, 2008, **112***,* 11996–12000.

21. A. T. Ward, Raman Spectroscopy of Sulfur, Sulfur-Selenium, and Sulfur-Arsenic Mixtures, *J. Phys. Chem.,* 1968, **72**, 4133-4139.

22. K. R. Loos and A. C. Jones, Structure of the Triiodide Ion in Solution. Raman Evidence for the Existence of Higher Poly Iodide Species, *J. Phys. Chem.,* 1974, **78**, 2306-2307.

23. W. Kiefer and H. J. Bernstein, Vibrational-Rotational Structure in the Resonance Raman Effect of Iodine Vapor, *J. Mol. Spectrosc.*, 1972, **43**, 366-381.

FIGURE CAPTIONS

Figure 1. (A) Schematic diagram of the quartz-made reactor cell. The actual cell dimensions are described in section 2.1; (B) Diagram of the T-shape construction showing the reactor cell containing the NaI/H_2O solution attached to the vacuum line. Valves 1 and 2 are also shown. The volume of the shaded area is 62 mL. Gaseous SO_2 introduced therein at a known pressure measured by the pressure indicator (PI) is -after opening valve V2- condensed in the cell, which is immersed in liquid nitrogen. The cell is then sealed by a propane-oxygen torch.

Figure 2. Actual photograph of the sealed cell containing the $I^-/H_2O/SO_2$ liquid under gaseous SO_2 at room temperature ($P_{SO_2,\,293\,K} = \sim 3.5 - 4$ bar) with I^-/H_2O =0.780 mol%, featuring the liquid separation into two conjugate phases. The green line portrays iconically the 532 nm laser irradiation of (a) the lower (SO_2-rich) phase; (b) the upper (iodide solution – rich) phase; and (c) the gas phase.

Figure 3. Raman spectra obtained for $I^-/H_2O/SO_2$ liquid mixtures in equilibrium with gaseous SO_2 at room temperature ($P_{SO_2,\,293\,K} = \sim 3.5 - 4$ bar) with I^-/H_2O mol% ratios in the 0 – 0.780 range as indicated by each spectrum. The inset shows the Raman spectra of the two liquid phases in equilibrium for the liquid mixture with I^-/H_2O = 0.780 mol%. Laser wavelength, λ_0 = 532.0 nm; Laser power, w = 100 mW; resolution, 2 cm^{-1}.

Figure 4. Raman spectra obtained for the $I^-/H_2O/SO_2$ liquid mixture with I^-/H_2O = 0.156 mol%: (a) at 25 °C, just after the ex situ 30 min crash test at 125 °C and insertion into the Raman furnace; (b) At 118 °C, after 9.75 h of reaction time. Recording parameters: see the Fig. 3 caption.

View Article Online
DOI: 10.1039/D5CP02071A

Figure 5. Sequential *in situ* Raman spectra obtained for $I^-/H_2O/SO_2$ liquid reacting mixtures at 118 °C in the S – O stretching wavenumber region after reaction time duration as indicated by each spectrum. (A) I^-/H_2O = 0.156 mol%; (B) I^-/H_2O = 0.780 mol%. Recording parameters: see the Fig. 3 caption.

Figure 6. Sequential *in situ* Raman spectra obtained for the vapors over $I^-/H_2O/SO_2$ liquid reacting mixtures in the 0.75 – 9 h reaction time span. (A) I^-/H_2O = 0.156 mol%; (B) I^-/H_2O = 0.312 mol%; (C) I^-/H_2O = 0.469 mol%. Recording parameters: see the Fig. 3 caption.

Figure 7. (A) Plots of the SO_2 pressure determined by exploiting the Raman band intensities of the $\nu_1(SO_2)$ mode (see experimental section) as a function of reaction time for the reactor batches with: (a) I^-/H_2O = 0.156 mol%; (b) I^-/H_2O = 0.312 mol%; (c) I^-/H_2O = 0.469 mol%; I^-/H_2O = 0.780 mol%.

(B) Plots of the average percent hourly SO_2 consumption rates as a function of reaction time for the reactor batches with: (a) I^-/H_2O = 0.156 mol%; (b) I^-/H_2O = 0.312 mol%; (c) I^-/H_2O = 0.469 mol%; I^-/H_2O = 0.780 mol%.

Figure 8. (A) Photograph of the reactor cell with I^-/H_2O = 0.156 mol% after 9 h of reaction time taken at room temperature. The yellow solid chunk can be seen at the bottom of the cell appendix containing the $H_2O/SO_2/I^-/HSO_4^-$ liquid mixture.

(B) Photograph taken through the window of he Raman furnace featuring the solid yellow chunk glowing due to focused irradiation by the 532.0 nm laser beam at a power of 5 mW.

(C) Raman spectrum obtained for the solid chunk contained in the $H_2O/SO_2/I^-/HSO_4^-$ liquid mixture at T=30 °C. Laser wavelength, λ_0 = 532.0 nm; Laser power, *w* = 5 mW; resolution, 2 cm^{-1}.

Figure 9. Raman spectra obtained for the $I^-/H_2O/SO_2$ liquid mixture with I^-/H_2O = 0.312 mol%: (a) at 25 °C, just after the ex situ 30 min crash test at 125 °C and insertion into the Raman

View Article Online
DOI: 10.1039/D5CP02071A

furnace; (b) At 25 °C, after 9 h of reaction time at 118 °C ; (c) At 25 °C, after a further shelf time of 32 days. Recording parameters: see the Fig. 3 caption.

Figure 10. (A) Sequential *in situ* Raman spectra obtained at 118 °C for the vapors over $I^-/H_2O/SO_2$ liquid reacting mixture with I^-/H_2O = 0.780 mol% in the 0.75 – 8.5 h reaction time span. Recording parameters: see the Fig. 3 caption.

(B) Raman spectra obtained at 118 °C for: (a) the vapors over the $H_2O/SO_2/I^-/HSO_4^-$ liquid mixture with I^-/H_2O = 0.780 mol% after 9 h of reaction time; (b) the $H_2O/SO_2/I^-/HSO_4^-$ liquid mixture after 10 h of reaction time. Recording parameters: see the Fig. 3 caption.

(C) Photograph of the reactor cell with I^-/H_2O = 0.780 mol% after 10 h of reaction time at 118 °C taken at room temperature. The purple iodine vapors fill the gas phase, whilst the product sulphur chunk is impregnated with iodine.

(D) Raman spectra obtained at 25 °C for the $H_2O/SO_2/I^-/HSO_4^-$ liquid mixture with I^-/H_2O = 0.780 mol% after 10 h of reaction time at 118°C. Recording parameters: see the Fig. 3 caption.

View Article Online
DOI: 10.1039/D5CP02071A

The data supporting this work are included in the main article and its Supplementary Information.

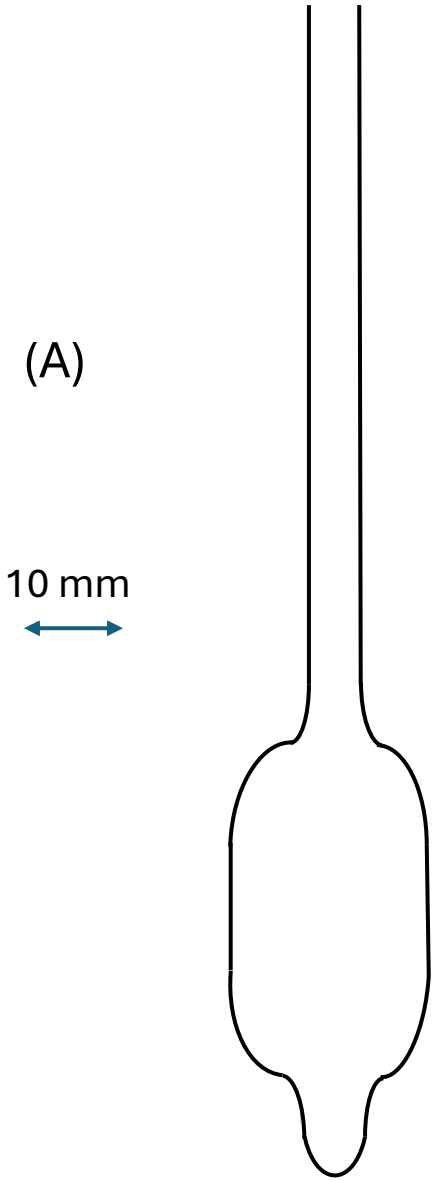

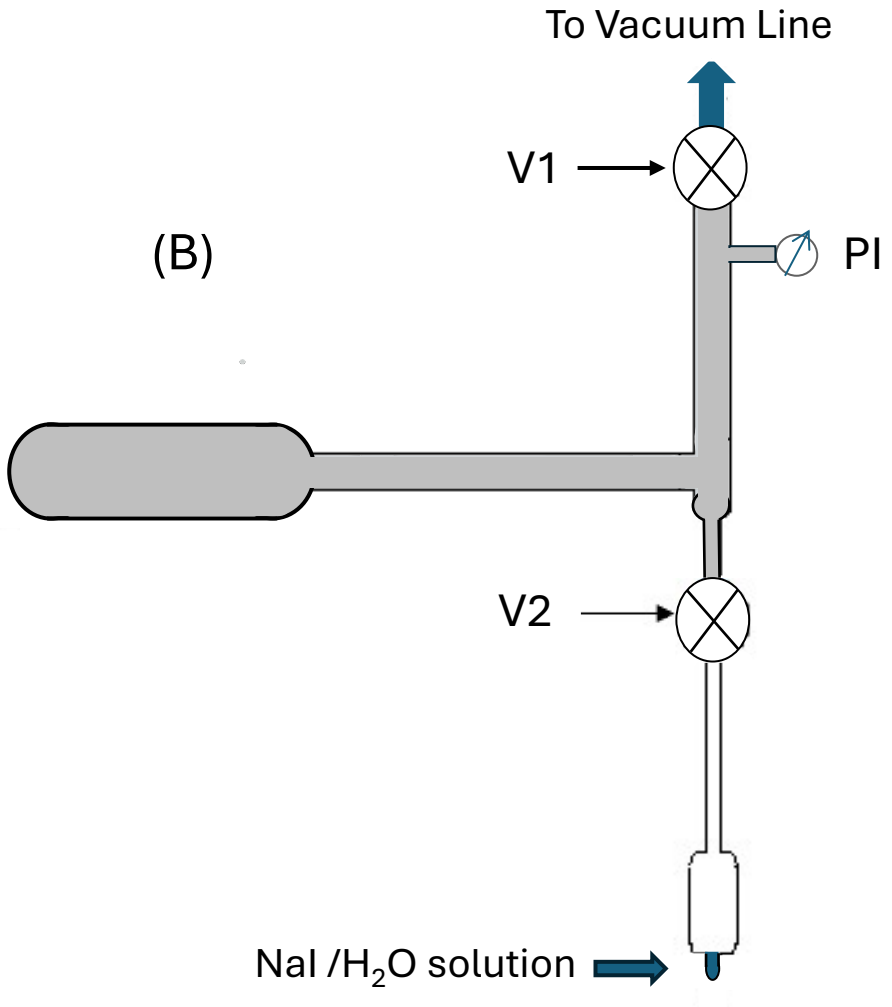

Figure 1

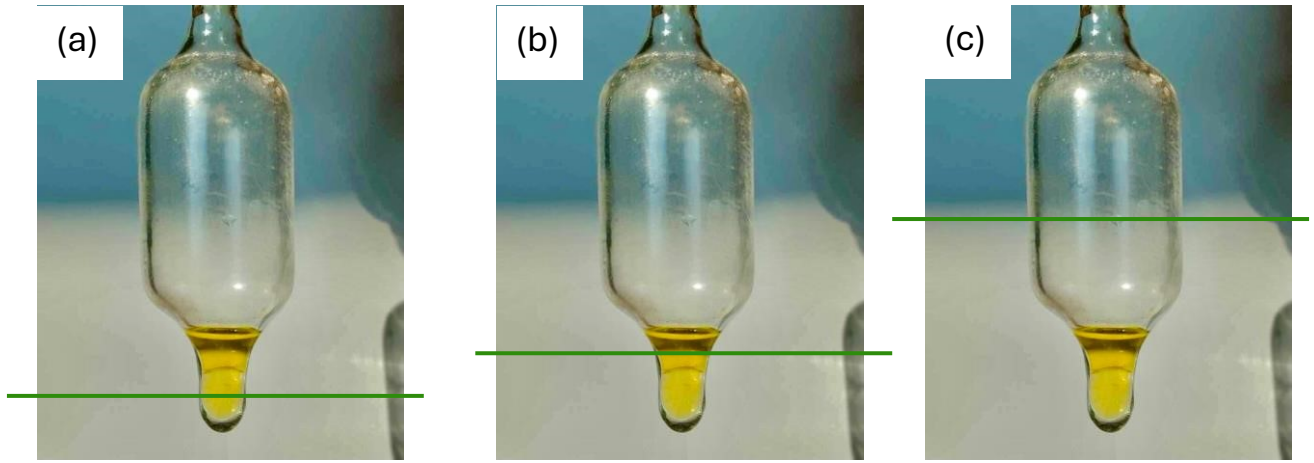

Figure 2

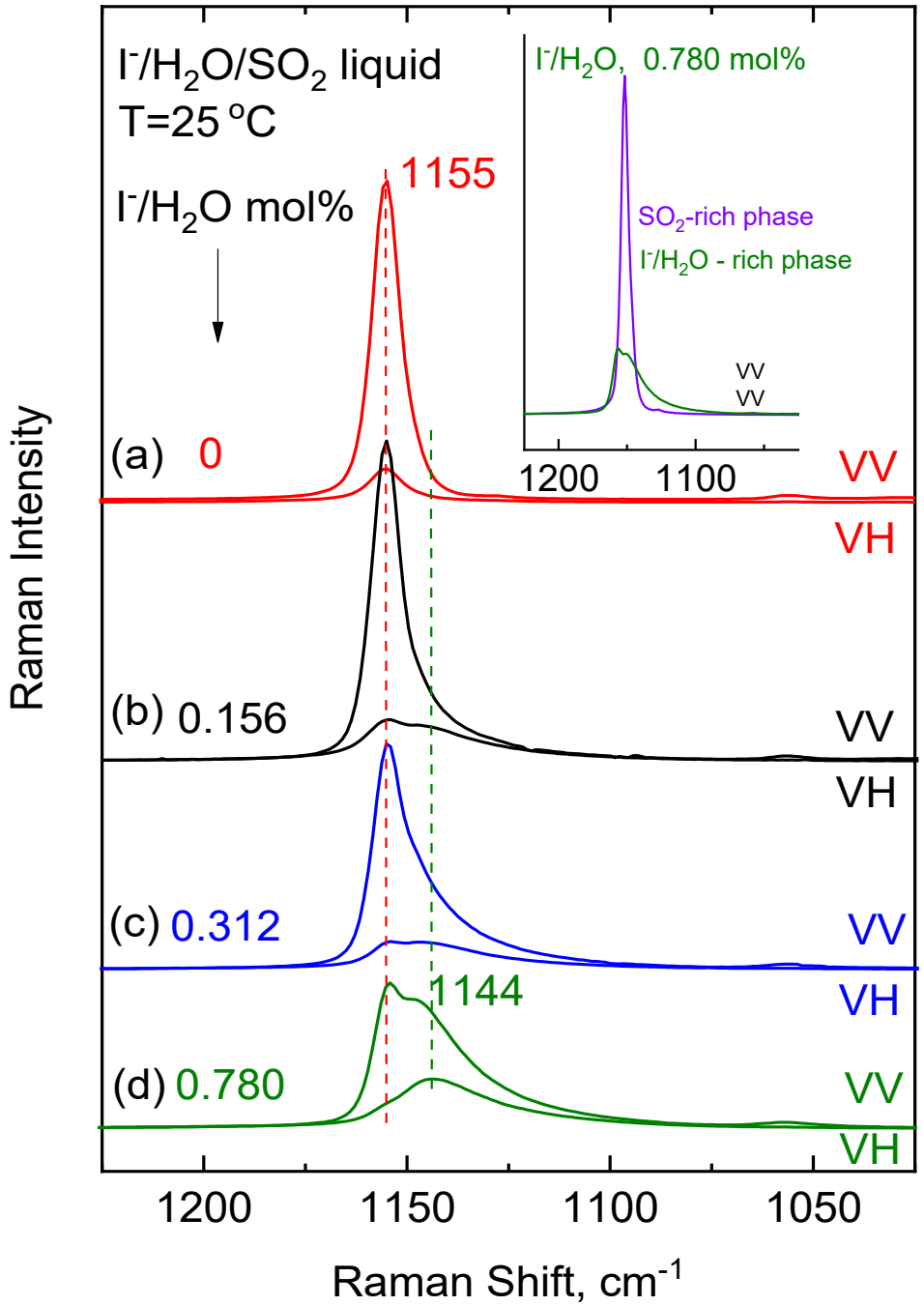

Figure 3

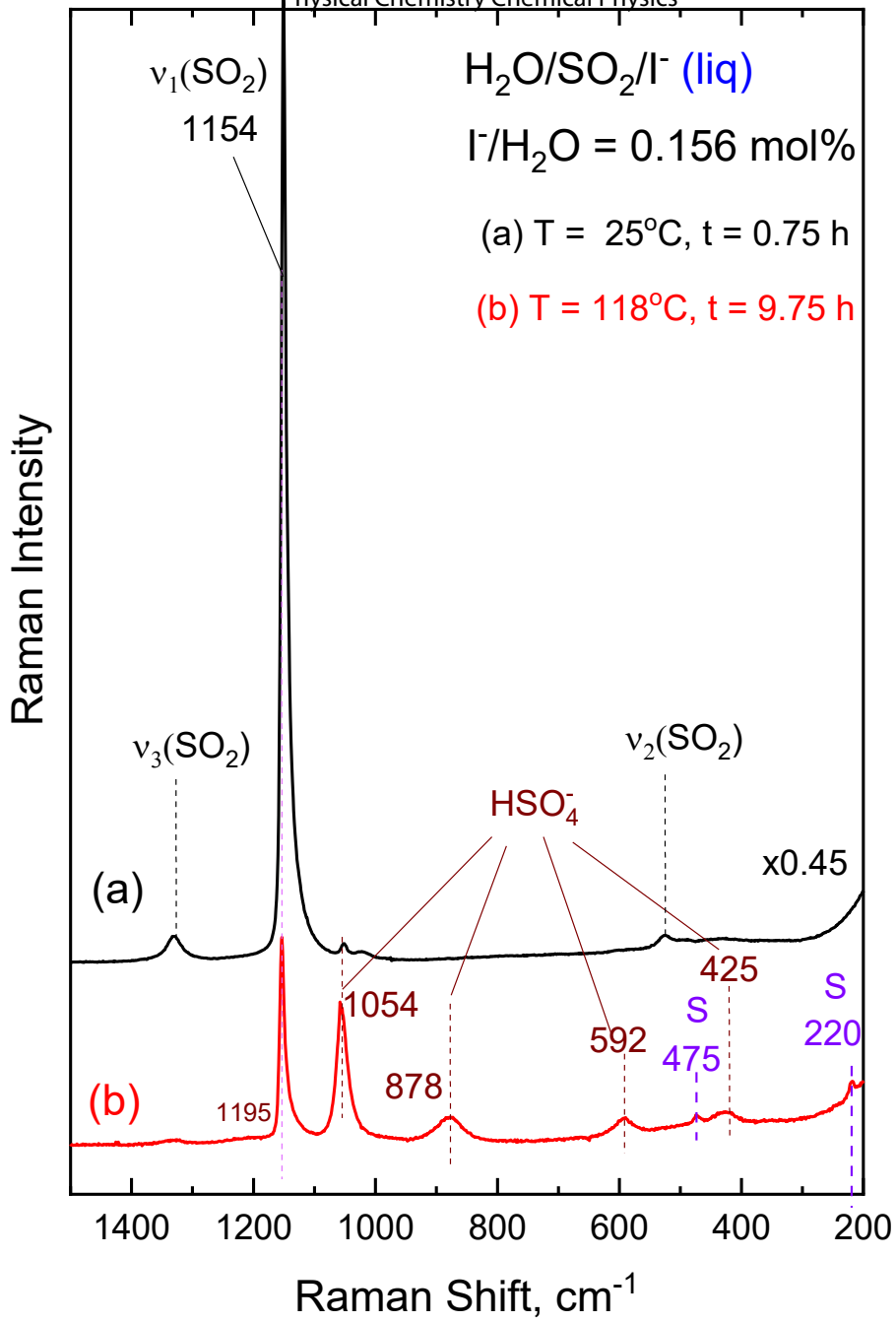

Figure 4

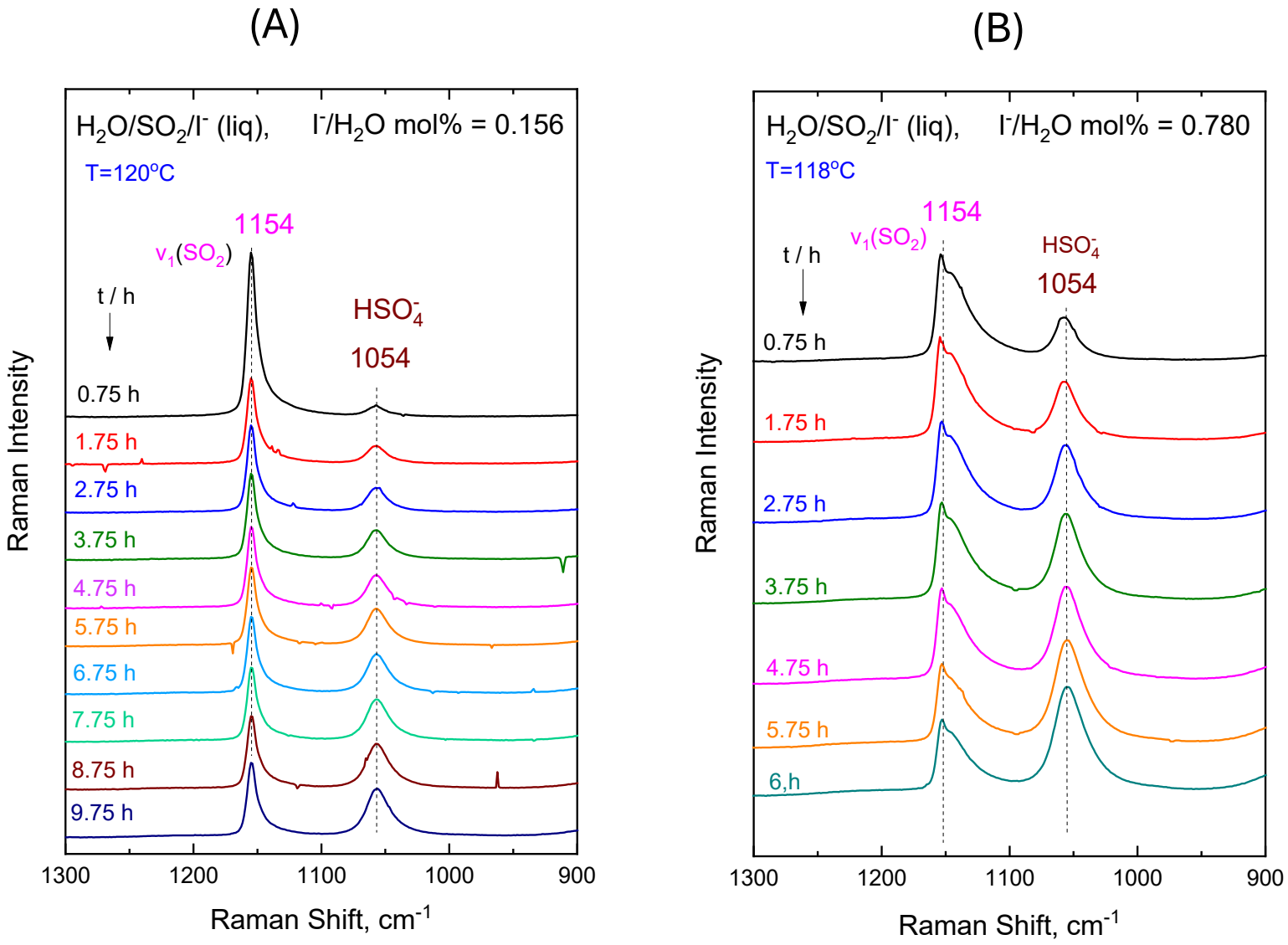

Figure 5

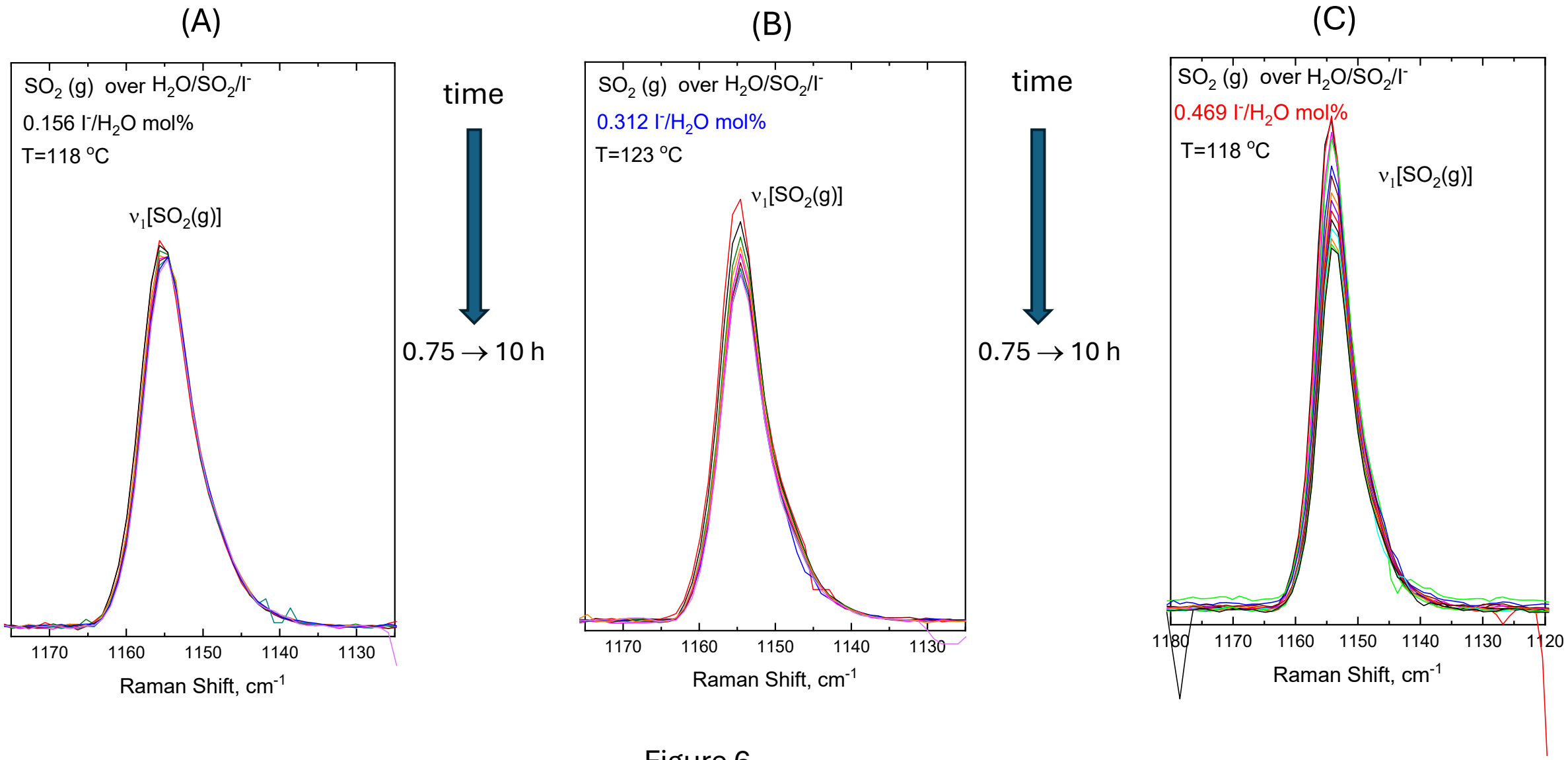

Figure 6

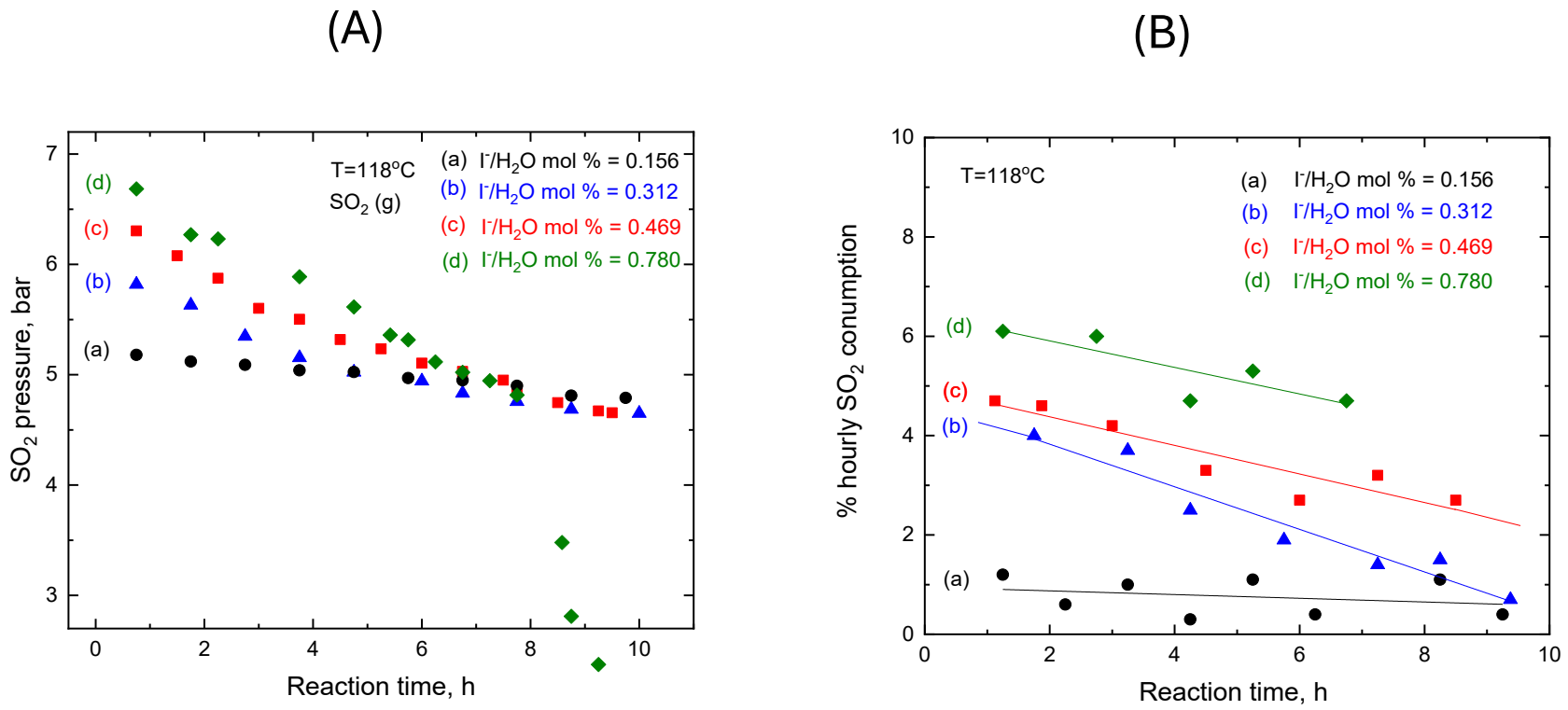

Figure 7

(A)

(B)

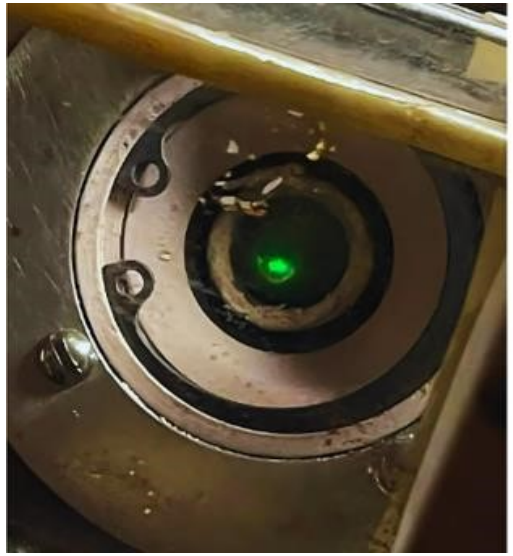

(C)

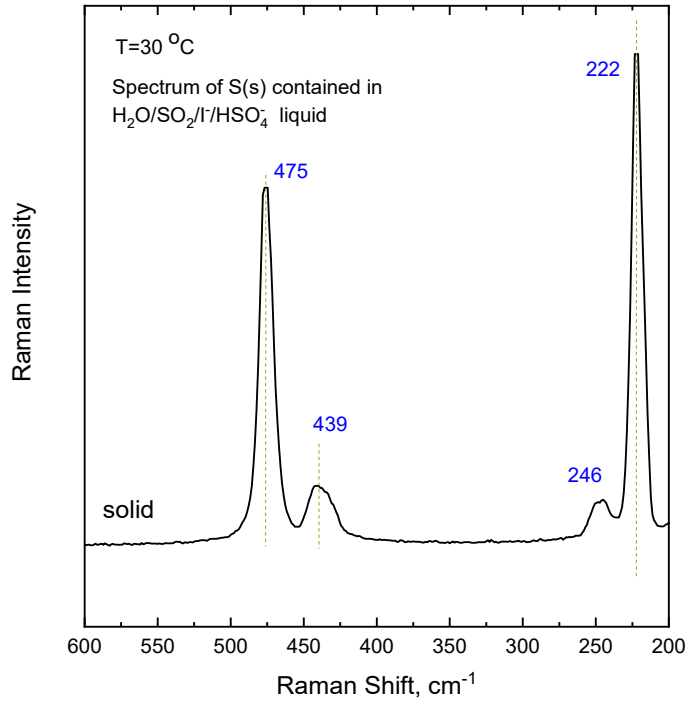

Figure 8

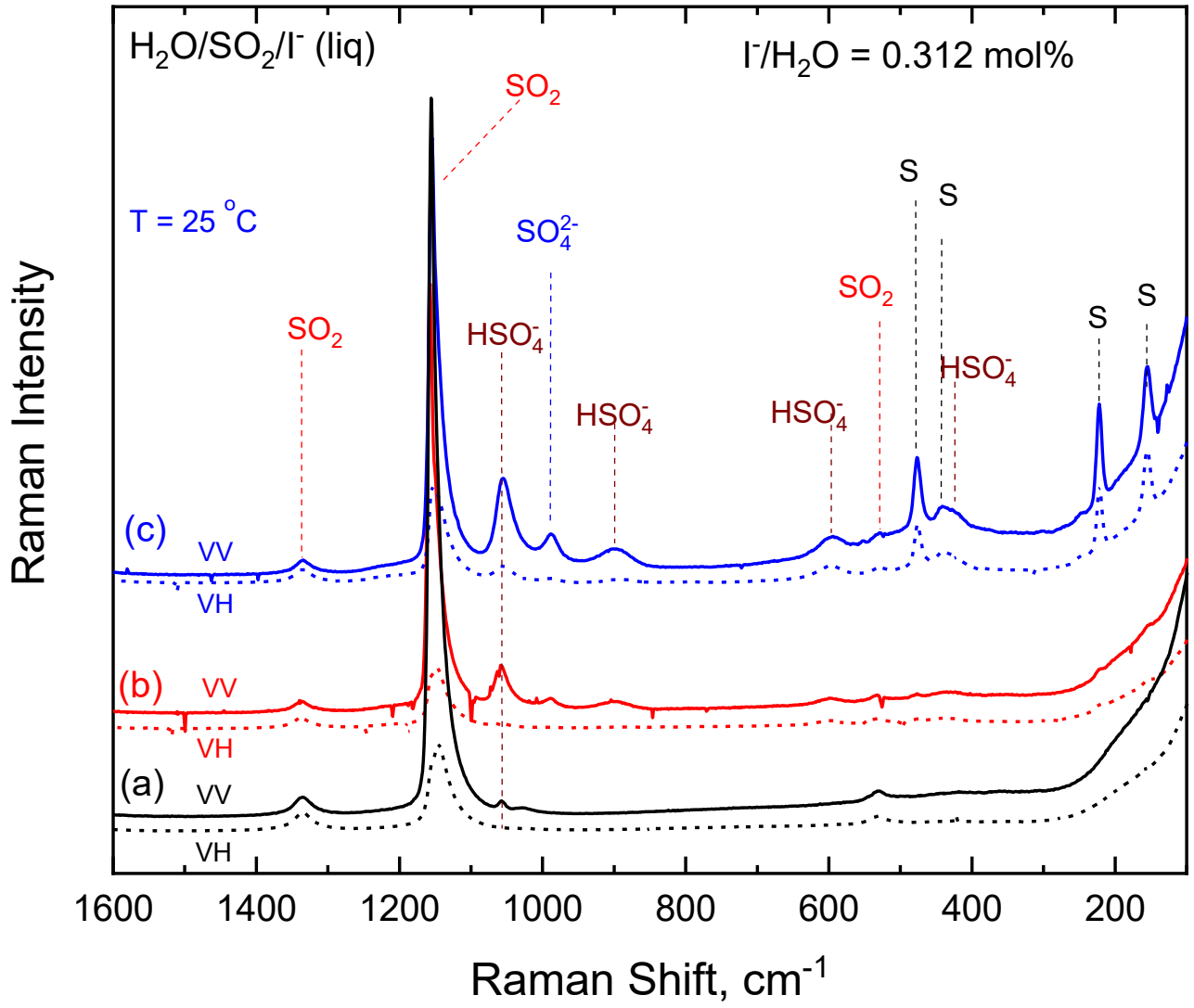

Figure 9

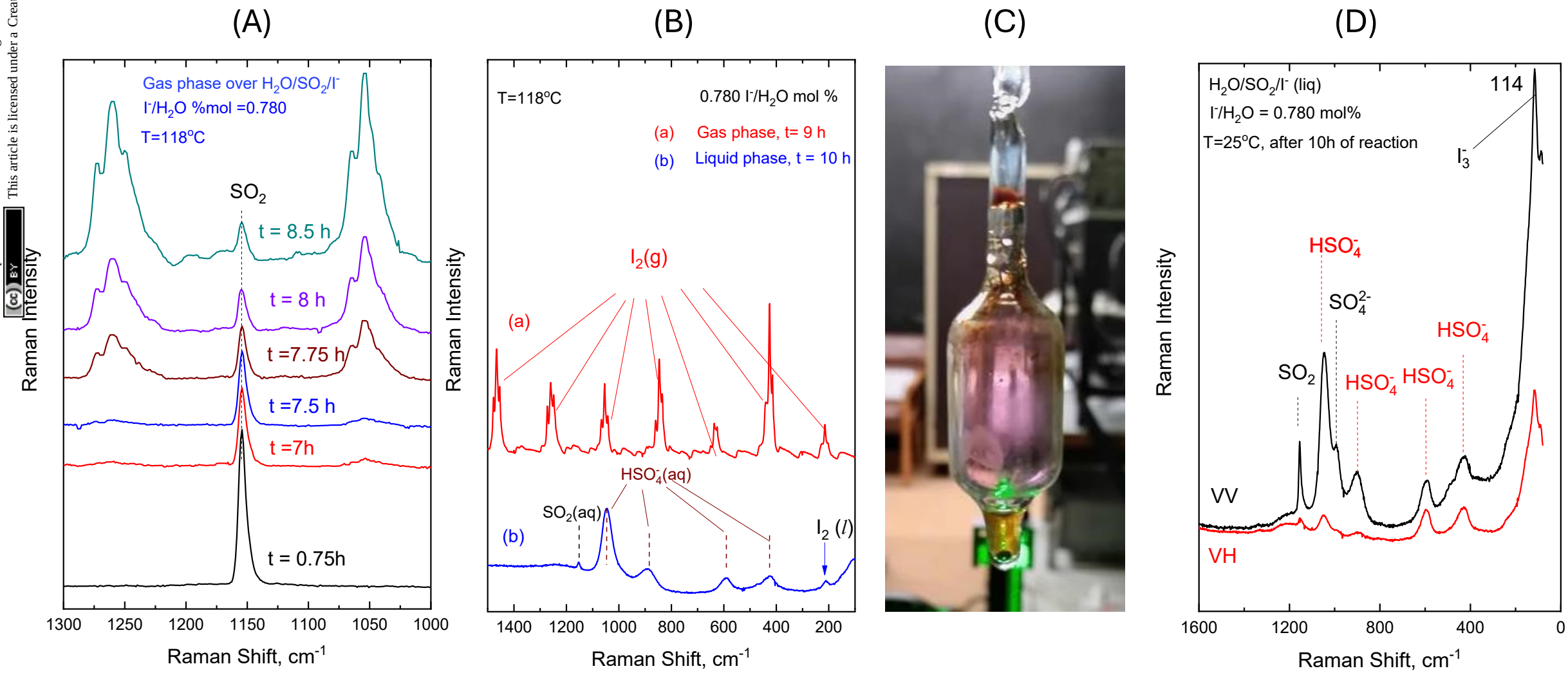

Figure 10